# The interior of Comet 67P/C-G; revisiting CONSERT results with the exact position of the Philae lander

Woldek Kofman, S. Zine, Alain Hérique, Y. Rogez, Laurent Jorda, Anny Chantal Levasseur-Regourd

Monthly Notices of the ROYAL ASTRONOMICAL SOCIETY

MNRAS **497,** 2616–2622 (2020) doi:10.1093/mnras/staa2001
Advance Access publication 2020 July 15

# The interior of Comet 67P/C–G; revisiting CONSERT results with the exact position of the Philae lander

Wlodek Kofman [1,2]★ Sonia Zine [1]★ Alain Herique [1] Yves Rogez,[1] Laurent Jorda[3] and Anny-Chantal Levasseur-Regourd[4]

[1] *Univ. Grenoble Alpes, CNRS, CNES, IPAG, F-38000 Grenoble, France*
[2] *Centrum Badan Kosmicznych Polskiej Akademii Nauk (CBK PAN), PL-00–716 Warsaw, Bartycka 18A, Poland*
[3] *Laboratoire d'Astrophysique de Marseille Pôle de l'Étoile Site de Château-Gombert,13388 Marseille, France*
[4] *Sorbonne Univ., CNRS, CNES, LATMOS, F-75005 Paris, France*

Accepted 2020 July 2. Received 2020 July 1; in original form 2020 April 23

## ABSTRACT

CONSERT, a bistatic radar onboard the *Rosetta* spacecraft and its Philae lander, was designed to probe the nucleus of comet 67P/Churyumov–Gerasimenko with radio waves at 90 MHz frequency. In 2016 September, the exact position of Philae was retrieved, within the region previously identified by CONSERT. This allowed us to revisit the measurements and improve our analysis of the properties of the interior, the results of which we present here**.** The relative permittivity of the materials is found to range from about 1.7 to 1.95 in the shallow subsurface (<25 m) and about 1.2 to 1.32 in the interior. These differences indicate different average densities between the shallow subsurface and the interior of comet. They can be explained by various physical phenomena such as different porosities, the possible compaction of surface materials, or even perhaps different proportions of the same materials. This strongly suggests that the less dense interior has kept its pristine nature.

**Key words:** techniques: radar astronomy – comets: general – comets: individual: 67P/Churyumov–Gerasimenko.

## 1 INTRODUCTION

CONSERT is a bistatic radar onboard both the *Rosetta* spacecraft and its lander Philae (Kofman et al. 2007), designed to probe the nucleus of comet 67P/Churyumov–Gerasimenko (hereafter 67P/C–G) in transmission. CONSERT's radio waves travel through the nucleus with a free space wavelength of about 3 m. The first measurements of the cometary interior were obtained by the CONSERT experiment during the *Rosetta* mission, and provided the dielectric properties and the internal structure of the small lobe, as well as the first estimation of the lander position (Ciarletti et al. 2015; Herique et al. 2015; Kofman et al. 2015; Herique et al. 2016; Ciarletti et al. 2017). In 2016 September, the exact position of the Philae lander was imaged and retrieved, coinciding with the region on the comet surface identified by CONSERT. This allowed us to revisit the interpretation of CONSERT measurements and to improve our analysis of the properties of the interior of the comet**,** which is the objective of this paper. We analysed the propagation paths of rays inside the comet, studying their length, depth, and propagation time through the nucleus. We discovered that rays propagating in the shallow subsurface have smaller velocities than those propagating in the deeper interior. This means that the permittivities are different, with the shallow subsurface showing larger permittivity values (∼ 2) than the deep interior (∼ 1.27), close to the values found previously by Kofman et al. (2015). These differences likely indicate varying densities between the shallow subsurface (<about 25 m) and the interior of the small lobe of comet 67P/C–G. These can be explained by a variety of physical phenomena, such as differences in the porosities of the two media, possible compaction and/or recondensation of surface materials, or perhaps a mixture of different proportions of the same materials in each medium.

★ E-mail: wlodek.kofman@univ-grenoble-alpes.fr (WK); sonia.zine@univ-grenoble-alpes.fr (SZ)

## 2 METHODS

### 2.1 General description

The CONSERT instrument measured the signals that propagated through the portion of 67P/C–G that stands between the Philae lander and the *Rosetta* spacecraft. The main observed parameters by this radar experiment are the propagation time and the amplitude of the signal at given orbital positions of the *Rosetta* spacecraft. To determine paths inside the comet, we used 3D modelling of the signal's propagation through the comet. In our models, the radar signal from the lander to the *Rosetta* spacecraft on its orbit was propagated using the latest stereophotoclinometric shape model of the comet (SPC shap8 v2.1) with 12 M facets, a ray-tracing method (Born & Wolf 1970), and the refraction on the surface of the comet. We initially assumed homogeneous dielectric properties for the entire sounded area of the cometary interior (Kofman et al. 2015). In the simulations, the Philae lander is located on the surface near the coordinates derived from the 2016 September observations (O'Rourke et al. 2019). Because our simulations depend strongly on the local environment of the lander, we used OSIRIS (Keller et al. 2007; Jorda et al. 2016) and NAVCAM images of the landing site,

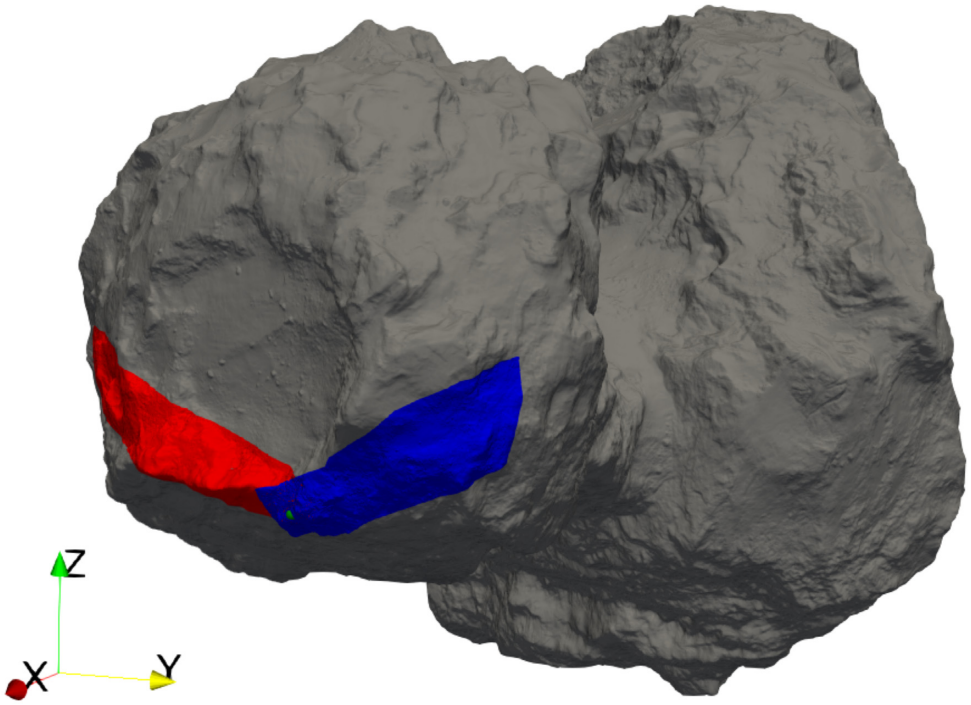


**Figure 1.** Measurement regions. The evening measurement (red) and the morning measurement (blue) of the area of the cometary head sounded by CONSERT.

available from the Planetary Science Archive (PSA) of ESA, to select the lander location on the shape model that best reflects the local slopes of the actual landing site. This location for the simulations is 13 m away from the OSIRIS location given in the PSA data base (O'Rourke et al. 2019). However, considering the lateral sampling of ∼4 m on average (which can reach up to 10 m locally), the slight differences between the local ESOC (European Space Operations Centre) and Cheops/OSIRIS frames, and the differences between the shape models in use, this difference in the lander location is acceptable (Jorda et al. 2016; O'Rourke et al. 2019).

We determined the paths for which the measured and simulated signals had the best matching propagation times. A match is obtained by adjusting the dielectric properties of the cometary interior and minimizing the quadratic distance between the calculated and the measured propagation times (Kofman et al. 2015). We use a similar method to that in Kofman et al. (2015), however, at the time of that study the exact position of the lander was still unknown. We knew only the approximate area (150 by 15 m) of the probable landing site location (Herique et al. 2015; Kofman et al. 2015), which meant we had to fit the lander position as an additional parameter to the permittivity determination. Therefore, we were only able to determine the average dielectric properties of the interior without knowing the propagation paths exactly**.** The resulting position of the lander was then close to the real one, but not exactly the same.

In the present analysis, the output of the simulations is the signal paths inside the comet and their lengths and depths, which are calculated in terms of the closest distance to the surface. The calculations of depths were done for every metre on the path of the rays**,** and then we found the distribution (occurrences) of each of the depth measurements, and the maximum and mean depths, the minimum being of zero. The unexpected final configuration of Philae on the nucleus surface introduces too many uncertainties on our knowledge of the CONSERT antenna gain. Knowledge of the digital model of the landing site and the exact configuration of the lander within the surrounding region are not good enough to calculate the precise antenna gain. To do so, we would need a digital model with a submetric resolution of the lander antenna's surroundings. Therefore, we did not use the amplitudes of signals as parameters to constrain paths.

In this article, we identify areas where the signals propagated and the places from which signals left the nucleus and propagated to the spacecraft. We determined a limited number of areas and propagation paths**,** and found the best matching permittivities.

### 2.2 Determination of observed and simulated paths inside the comet

On 2014 November 12th, CONSERT operated during two periods with very good data quality and a high signal-to-noise ratio; the first measurement sequence was during the evening (on Earth at about 19:00 UTC)**,** and the second during the morning (about 02:00 UTC on Earth). These two periods corresponded to two opposite directions of the propagation through the head of the comet presented in Fig. 1; the first one to the West ( through the Hatmehit, Wosret, and Maftet regions defined by El-Maarry et al. 2017), and the second one to the East (Bastet region). This has an effect on the signal's amplitude, due to the orientation of the lander on the surface. The CONSERT instrument was built to maximize the amplitude of the signals by matching the polarizations between the Rosetta and Philae antennas, assuming that the lander would send signals directed towards the bottom of its own antenna. The propagation during morning measurements is in the direction of the lander $+z$-axis, which is oriented towards the top of the lander antenna, while the propagation during evening operations is mostly in the $-z$ direction. This implies that the polarization is opposite in both measurement sequences. The matched polarization between lander and orbiter antennas is in the $-z$ direction. Therefore, the signal measured during

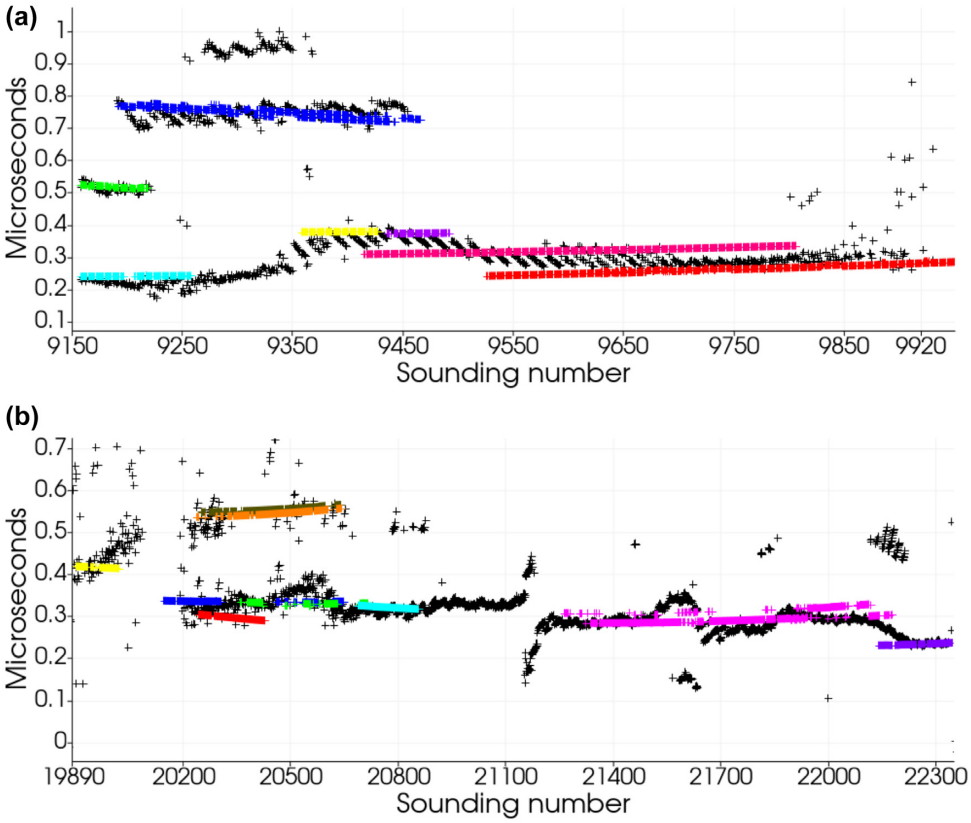


**Figure 2.** Propagation time. The propagation time measurements (crosses) of different paths identified for the 'evening' measurements (a) and for the 'morning' (b) compared to those from simulations (colours). Colours indicate the identified areas respectively in Figs 3(a) and (b)**,** in which the spots where the rays exit the comet towards the *Rosetta* spacecraft are shown. The permittivity corresponding to each area is given in Tables 1 and 2, respectively (colour indicated in column 2).

the evening operations should be lower than the one measured in the morning**.** Indeed, this was observed in Kofman et al. (2015).

In the simulations, we generate wavefronts as sets of rays that have propagations paths and times that are close to one another, arrive in the same sector on the Rosetta orbit, and leave the comet from the same area on the surface with respect to the signals' wavelength. Then, we compare them with the measured propagation time of the observed signals, choosing the best matching solutions. In Figs 2(a) and (b), we compared the measured and simulated propagation times and plotted them in different colours for the two measurement sequences, respectively.

These figures show the quality of convergence between measurements and simulations by adjusting the permittivities.

The colours correspond to areas from which signals exited the comet (spots in Fig. 3 at the ends of traced rays, numbered and in colour), and were transmitted to the orbiter (Figs 4a and b, with coloured rays propagating in vacuum, coloured with the same colour scheme as the numbers of spots in Fig. 3).

In Fig. 3, we also plot the part of the cometary head through which signals propagated. The colour of the ray traces plotted on the surface indicates the distance from these rays to the surface for each ray identified inside the nucleus.

## 3 RESULTS

The calculated parameters for each area are indicated in Tables 1 and 2. The rays that reach the orbiter exit the nucleus from a few limited areas. In these tables, we show the average parameters of the rays that correspond to wavefronts evaluated separately for each area.

Within the evening measurements, seven areas were studied. The signals propagated along distances ranging from ∼250 to ∼1170 m inside the nucleus at depths varying from deep (∼150 m) to shallow (∼15 m). Only one path (area 6, cyan) corresponds to a shallow depth with a short length (250 m) inside the nucleus.

Within the morning measurements, some signals propagated with long paths (∼560 to ∼850 m) and maximal depths within the comet between ∼50 and ∼110 m, and others with short (250 m) and shallow propagation paths with maximal depths of ∼30 to ∼40 m.

### 3.1 Dielectric properties of the nucleus interior

In the tables, we summarize the average permittivities that correspond to the best matching propagation time for each area separately. Results are different for the deep propagations and for the shallow ones. For the former, with a mean depth larger than about 20 m, which is seen in Table 2, the average permittivity is about 1.30 and for the latter the average permittivity is more than 1.5. These results tend to show a variation of the permittivity as a function of the mean depth through which the corresponding wavefront travelled inside the nucleus. This leads us to define two zones, shallow and deep, for which we determine the permittivities and the depth of the first zone by minimizing the quadratic errors between the measured and predicted permittivities.

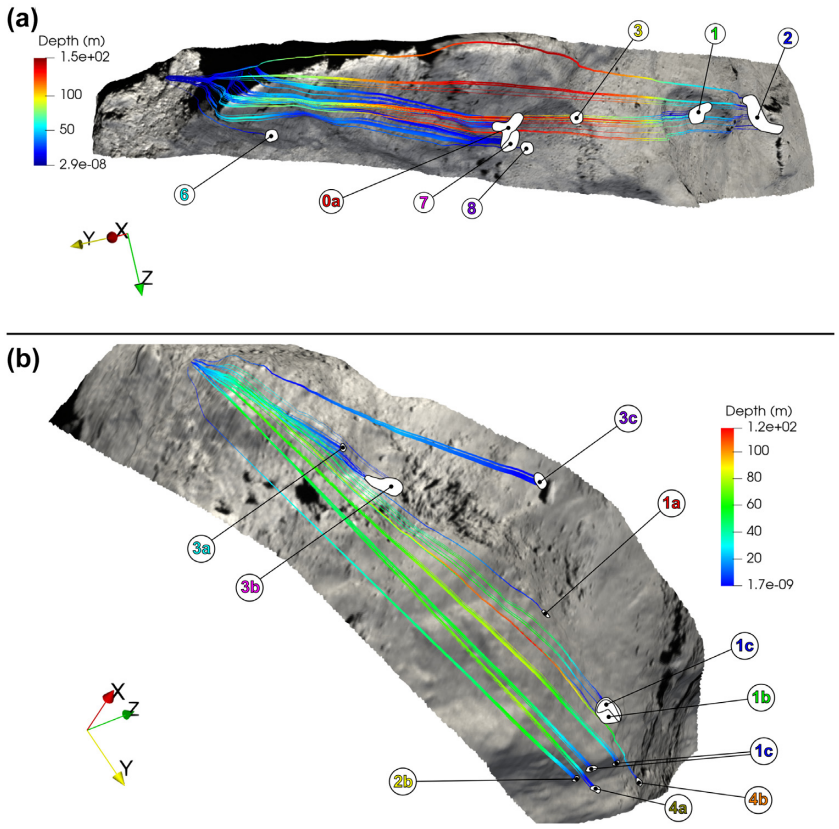


**Figure 3.** Rays and their depths. The 'evening' (a) and 'morning' (b) ray traces plotted on the surface of the comet, indicating the explored zones. The colours of the traces indicate the distance from the surface (column 'depth' in tables) for each ray measured by CONSERT. The coloured numbers of the spots on the surface are those of the wavefronts in Figs 2(a) and (b), and those of the rays going out from the comet to the *Rosetta* spacecraft are shown in Fig. 4. The permittivity of each area is indicated in column 3 of the tables. Each area is seen here as a spot on the surface. The lander is located on the left end of this figure.

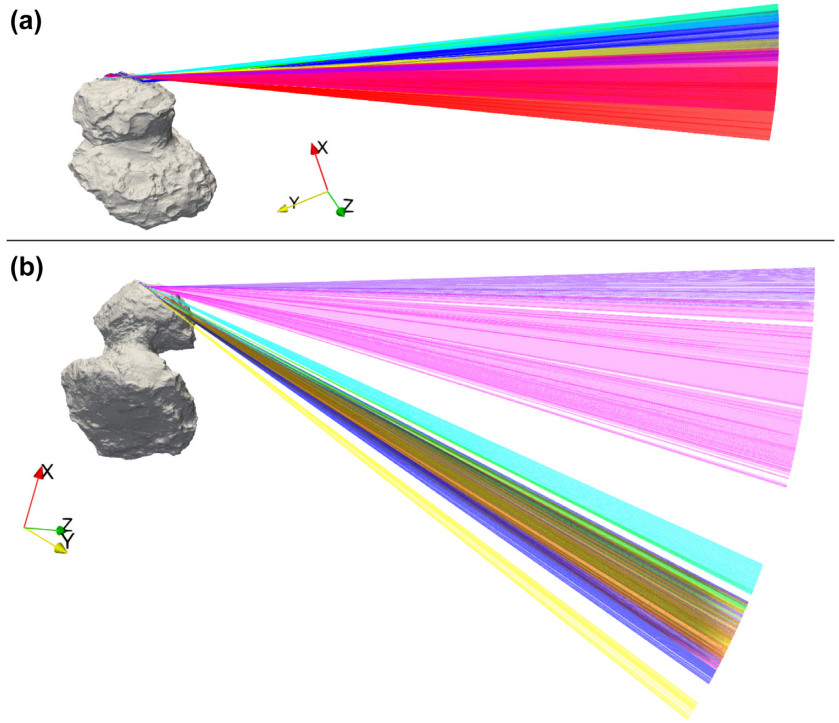


**Figure 4.** Rays propagating to *Rosetta*. The simulated wavefronts leaving the comet and arriving on the orbit positions of *Rosetta* for the 'evening' (a) and for the 'morning' (b). The image presents the comet and orbit from the left and right sides. The colours correspond to the different wavefronts in Tables 1 and 2.

**Table 1.** Evening measurement.

| Area | | Permittivity | Relative propagation time (μs) | | | Distance inside (m) | | | Depth (m) | |
|---|---|---|---|---|---|---|---|---|---|---|
| ID | Colours | Epsilon | min | max | mean | min | max | mean | max | mean |
| 0a | Red | 1.29 | 0.26 | 0.31 | 0.28 | 410 | 500 | 478 | 54 | 21 |
| 1 | Green | 1.29 | 0.51 | 0.52 | 0.52 | 1011 | 1017 | 1013 | 123 | 65 |
| 2 | Blue | 1.37 | 0.72 | 0.78 | 075 | 1156 | 1201 | 1172 | 154 | 77 |
| 3 | Yellow | 1.32 | 0.38 | 0.38 | 0.38 | 755 | 755 | 755 | 65 | 35 |
| 6 | Cyan | 1.50 | 0.24 | 0.24 | 0.24 | 253 | 254 | 254 | 41 | 15 |
| 7 | Pink | 1.29 | 0.31 | 0.34 | 0.32 | 660 | 667 | 664 | 64 | 24 |
| 8 | Violet | 1.35 | 0.38 | 0.37 | 0.37 | 667 | 667 | 667 | 65 | 23 |

**Table 2.** Morning measurements.

| Area | | Permittivity | Relative propagation time (μs) | | | Distance inside (m) | | | Depth (m) | |
|---|---|---|---|---|---|---|---|---|---|---|
| ID | Colours | Epsilon | min | max | mean | min | max | mean | max | mean |
| 1a | Red | 1.30 | 0.29 | 0.30 | 0.30 | 562 | 563 | 563 | 51 | 21 |
| 1b | Green | 1.29 | 0.32 | 0.33 | 0.33 | 689 | 723 | 718 | 67 | 43 |
| 1c | Blue | 1.26 | 0.33 | 0.34 | 0.3 | 721 | 807 | 767 | 83 | 45 |
| 2b | Yellow | 1.30 | 0.42 | 0.44 | 0.43 | 693 | 819 | 785 | 86 | 41 |
| 3a | Cyan | 1.86 | 0.32 | 0.33 | 0.32 | 240 | 242 | 242 | 38 | 19 |
| 3b | Pink | 1.75 | 0.28 | 0.30 | 0.29 | 244 | 257 | 251 | 42 | 18 |
| 3c | Violet | 1.86 | 0.23 | 0.24 | 0.23 | 125 | 126 | 126 | 30 | 10 |
| 4a | Brown | 1.40 | 0.55 | 0.56 | 0.55 | 800 | 802 | 801 | 78 | 45 |
| 4b | Orange | 1.40 | 0.54 | 0.56 | 0.54 | 870 | 872 | 871 | 117 | 69 |

*Notes*. Tables 1 and 2: The colours (column 2) indicate rays exiting the comet towards the *Rosetta* spacecraft from a given identified area (column 1); they correspond to the spots and rays in Figs 2–4. We indicate the estimated permittivities (epsilon, column 3); the minimum, maximum, and mean propagation times relative to the direct propagation time from lander to orbiter in vacuum (columns 4, 5, and 6); the maximum, minimum, and mean distances travelled by the rays inside the comet in our simulations (columns 7, 8, and 9); and the maximum and mean depths (distance from the surface; columns 10 and 11). All parameters were calculated by averaging rays that correspond to single wavefronts in each area separately.

To do this, we calculated the number of occurrences of a depth ($d$) sampled at every metre segment along the propagation path for a set of rays in each zone that corresponds to the same wavefront; Pr($d < D$) is the fraction of occurrences (total occurrences normalized to one) of ray segments at a depth ($d$) smaller than $D$. This dichotomy depth defines two zones, which we take into consideration for the following analysis. For a given length of the propagation path inside the comet, this outputs the proportional time during which the signal was present at a depth smaller than $D$. With this statistic, we built the model that must be minimized to determine the interior's dielectric parameters. The propagation time inside the comet is composed of two parts; the propagation times in the first shallower zone and the propagation time in the second deeper zone, leading to the following equation (1):

$$\sqrt{\varepsilon_{\rm m}} = \Pr(d < D) * \sqrt{\varepsilon_1} + \Pr(d > D) * \sqrt{\varepsilon_2}, \quad (1)$$

where $\varepsilon_{\rm m}$ is the predicted permittivity, $\varepsilon_1$ and $\varepsilon_2$ are, respectively, the permittivity values of the first and second zones, and D is the thickness of the first zone.

We minimize the quadratic error between the measured $\varepsilon_{\rm M}{}^*$ and the $\varepsilon_{\rm m}$ predicted by the equation (1), varying three parameters ($\varepsilon_1$, $\varepsilon_2$, D), and using all 16 measurements of $\varepsilon_{\rm M}{}^*$ corresponding to all the areas. The uncertainty on $\varepsilon_{\rm M}*$ depends on the length of the path inside the comet and is about 0.1 for the short lengths (see appendix). In Figs 5(a), (b), and (c), we show the isodensity plots of the fitting error as a function of $\varepsilon_1$ and $\varepsilon_2$ for a fixed depth, and the isodensity plots of the fitting error as a function of permittivity $\varepsilon 1$ ($\varepsilon 2$) and depth for fixed values of $\varepsilon 2$ ($\varepsilon 1$). The final parameters are defined by the minimum value of the error. The minimum error dependent on the depth is a rather wide function**,** and gives optimal depth values between 14 and 25 m. The optimal $\varepsilon_1$ is between 1.7 and 1.95 and $\varepsilon_2$ is between 1.2 and 1.32 (Fig. 5).

These results for the second zone below ∼25 m are close to the values obtained by Kofman et al. (2015), with the difference that**,** until 2016, the exact position of the lander was not known, so we had to minimize the mean square root distance between the propagation times in simulations and measurements by also varying the position of the lander. Now, the lander coordinates are known with sufficient accuracy, so we need only iterate permittivity values in the simulations.

This important result shows the difference that exists between permittivity values of a shallow subsurface down to ∼25 m and a deeper interior of the comet. We do not claim here that a layered structure exists, rather, we define a depth scale at which the material properties change (see conclusions). The permittivity of the shallow subsurface is close to measurements published previously that show that the permittivity of the surface is approximately 2.0 [with a depth of the order of a metre for the Permittivity Probe (PP) on the Philae lander (Lethuillier et al. 2016), and decimetres to 2.5 m measured through Earth-based observation from Arecibo (Kamoun et al. 2014)].

## 4 CONCLUSIONS AND DISCUSSION: IMPACT OF THESE RESULTS ON THE COMETARY MODEL

The main result of the present analysis is the observed variability of the dielectric properties with depth within the cometary interior. We conclude that**,** close to the surface, for depths ranging from about 14 to 25 m, the permittivity values are between 1.7 and 1.95. Below, for depths between 25 and 150 m the permittivity is lower, with values

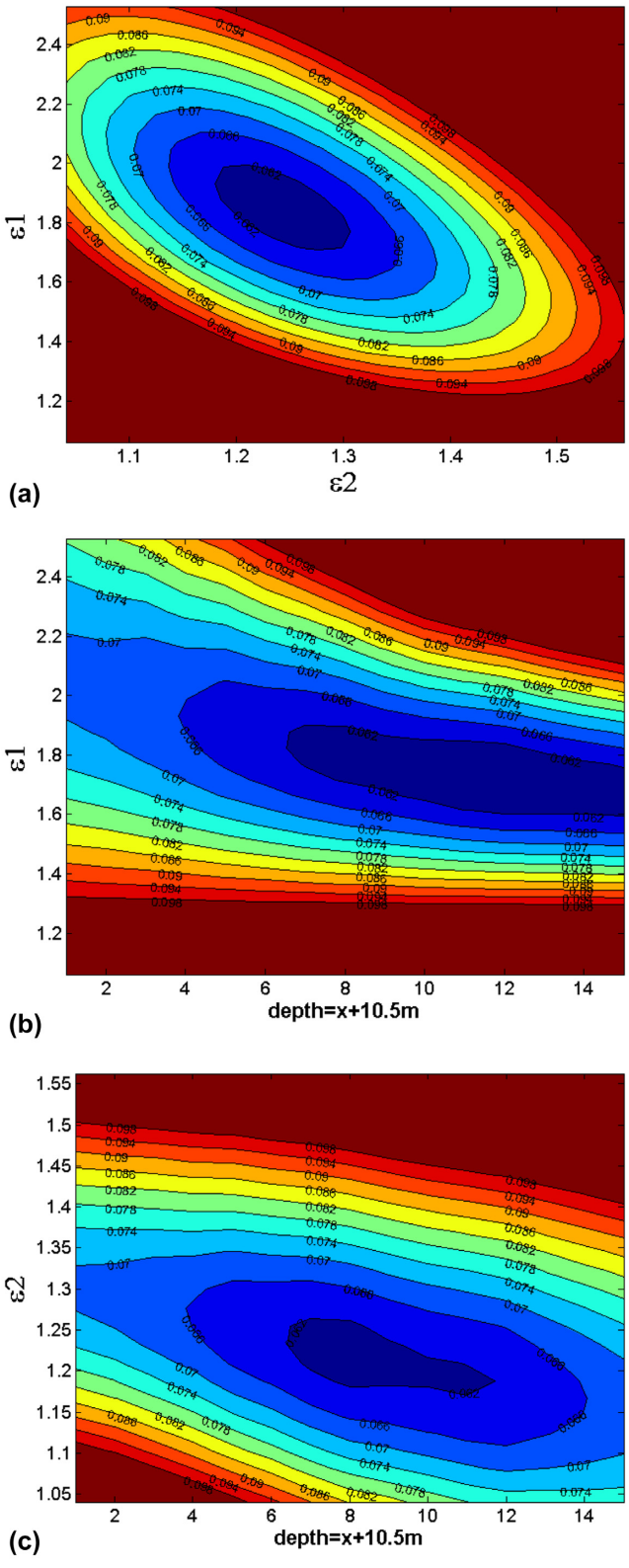


**Figure 5.** Fitted permittivities and their depths. (a) The isodensity of the fit error as a function of permittivity of the first ($\varepsilon 1$) and second ($\varepsilon 2$) depth zones, for a first depth zone of 18.5 m. (b) The isodensity of the fit error as function of the permittivity $\varepsilon 1$ and the depth of the first zone, for a fixed $\varepsilon 2 = 1.27$. (c) The isodensity of the fit error as a function of the permittivity $\varepsilon 2$ and the depth of the first zone, for a fixed $\varepsilon 1 = 1.9$.

between 1.2 and 1.32. The measurement of these dielectric properties of the cometary nucleus, is a completely new result. Thus far, only the first metre of the subsurface had been explored, either from Earth (Kamoun et al. 2014), or by the PP instrument (Lethuillier et al. 2016) on Philae. PP measurements were local to the close vicinity of Philae, and Arecibo measurements observed the comet globally and as a small target, without any spatial resolution. This variability with depth is an indication that the material that composes 67/P varies most likely from less porous near the surface (larger average density), to more porous in the deeper interior (i.e. average density decreases inward). This variation in porosity could be caused by a variety of different mechanisms. For example, it could indicate the possible compaction of the surface materials due to enhanced sublimation or recondensation of ices close to the surface, or it could mean the presence of different proportions of the same materials, which could imply composition changes to a higher dust-to-ice ratio close to the surface. In the interior part of the comet, the value of dust-to-ice ratio, does not change from the previous results and is larger than 3 (Choukroun et al. 2020).

A denser external zone is compatible with activity-induced effects such as the recondensation of water vapor near the surface (Skorov et al. 1999), which would decrease the porosity of the subsurface material. Additional mechanisms such as cliff collapses or the formation of dust deposits (El Maarry et al. 2019) may also play a significant role in getting more compact material to the surface.

The measurements of a thickness of 14–25 m for the external zone may be the result of such processes over repeated perihelion passes. However, erosion is responsible for the modification of the surface and of a shallow subsurface during each perihelion pass (El-Maarry et al. 2019), so this is likely to hinder the creation of a layered structure.

There is also the possibility of a smooth change of the permittivity with depth, as the compaction and the recondensation can act to increase or decrease the density of materials. Our measurements cannot uniquely explain the change in permittivity with depth, and they also cannot rule out the possibility of a smooth change in permittivity with depth.

These new results confirm that the subsurface is modified by its interaction with space, leading to the ejection of material that partially falls back on the nucleus (as extensively observed by OSIRIS). Our results also strongly suggest that the interior of the nucleus is more porous than its subsurface. It follows that its density is lower than the bulk density of the nucleus (about 533 kg $m^{-3}$; Jorda et al. 2016) in agreement with the low densities measured for ejected dust particles (Levasseur-Regourd et al. 2018). Such particles are indeed made up of porous agglomerates with very high porosity at the micrometre scale, as well as more compact aggregates (Güttler et al. 2019).

The porosity in the nucleus, corresponding to a permittivity of 1.27 and a bulk density of 533 kg $m^{-3}$, ranges from 73 to 76 per cent (Kofman et al. 2015; Herique et al. 2019), which is compatible with a model proposed that predicts very high porosities (>70 per cent) for the nucleus (Blum et al. 2017). For the lower values of the average density, corresponding values of porosity will be even larger.

As anticipated by M. A'Hearn in 2017 (A'Hearn 2017), 'the structure of the nucleus of 67P/C–G will ultimately lead to a better understanding of how cometary nuclei are assembled'. Indeed, CONSERT results are in favour of a scenario of formation of the small lobe of the nucleus by accretion in the protoplanetary disc around the Sun (Davidsson et al. 2016; Blum et al. 2017). It means that, as already suggested by A. H. Delsemme in 1977 (Delsemme 1977), 'Comets are likely to be the most pristine minor bodies in the Solar System'.

## ACKNOWLEDGEMENTS

CONSERT was designed, built, and operated by IPAG, LATMOS, and MPS, and was financially supported by Centre National d'Études Spatiales (CNES), Centre National de la Recherche Scientifique (CNRS), Université Grenoble Alpes (UGA), Deutsches Zentrum für Luft- und Raumfahrt (DLR), and Max Planck Institute for Solar System Research (MPS). Rosetta is an ESA mission with contributions from its Member States and NASA. Philae was provided by a consortium led by DLR, MPS, CNES, and Italian Space Agency (ASI).

Most of the computations presented in this paper were performed using the CIMENT infrastructure (https://ciment.univ-grenoble-alpes.fr), which is supported by the Rhône-Alpes region (GRANT CPER07_13 CIRA: http://www.ci-ra.org) and France-Grille (http://www.france-grilles.fr).

We are very grateful to the anonymous reviewer who helped us improve our manuscript.

## DATA AVAILABILITY

The Rosetta Navigation Camera description, https://imagearchives.esac.esa.int/index.php?/page/rosetta_Navcam.

CONSERT data are accessible on ESA's PSA archive.

## REFERENCES

A'Hearn M., 2017, Phil. Trans. R. Soc. A, 375, 20160261
Blum J. et al., 2017, MNRAS, 469, S755
Born M., Wolf E., 1970, Principles of Optics. Pergamon Press, New York
Choukroun M. et al., 2020, Space Sci. Rev., 216, 44
Ciarletti V. et al., 2015, A&A, 583, A40
Ciarletti V. et al., 2017, MNRAS, 469, S805
Davidsson B. J. R. et al., 2016, A&A, 592, A63
Delsemme A. H., 1977, in Delsemme A. H., eds, IAU Colloq., Comets, Asteroids, Meteorites: Interrelations, Evolution and Origins, Vol. 39. Cambridge University Press, Cambridge, p. 3
El-Maarry M. R. et al., 2017, A&A, 598, C2
El-Maarry M. R. et al., 2019, Space Sci. Rev., 215, 36
Güttler A et al., 2019, A&A, 630, A24
Herique A. et al., 2015, Planet. Space Sci., 117, 475
Herique A. et al., 2016, MNRAS, 462, S516
Herique A., Kofman W., Zine S., Blum J., Vincent J. - B., Ciarletti V., 2019, A&A, 630, A6
Jorda L. et al., 2016, Icarus, 277, 257
Kamoun P., Lamy P. L., Toth I., Herique A., 2014, A&A, 568, A21
Keller H. U. et al., 2007, Space Sci. Rev., 128, 433
Kofman W. et al., 2007, Space Sci. Rev., 128, 413
Kofman W. et al., 2015, Science, 349, aab0639
Lethuillier A. et al., 2016, A&A, 591, A32
Levasseur-Regourd A. C. et al., 2018, Space Sci. Rev., 214, 64
O'Rourke L. et al., 2019, Acta Astronaut., 157, 199
Skorov Y. V., Kömle N. I., Markiewicz W. J., Keller H. U., 1999, Icarus, 140, 173

## APPENDIX

The estimation of the error on the permittivity is given by the following equation:

$$T = \frac{s\sqrt{\varepsilon}}{c},$$

where $T$ is propagation time, $s$ is the length of the path inside the nucleus, $\varepsilon$ is permittivity, and $c$ is the velocity of light.

Therefore,

$$\left(\frac{\Delta\varepsilon}{\varepsilon}\right) = \frac{2\Delta T}{T} - \frac{2\Delta s}{s}$$

and

$$\left(\frac{\Delta\varepsilon}{\varepsilon}\right)^2 = 4\left(\frac{\Delta T}{T}\right)^2 + 4\left(\frac{\Delta s}{s}\right)^2$$

and finally

$$\left(\frac{\Delta\varepsilon}{\varepsilon}\right)^2 = 4\left(\frac{\Delta T c}{s\sqrt{\varepsilon}}\right)^2 + 4\left(\frac{\Delta s}{s}\right)^2.$$

For a short travel distance inside the nucleus, e.g. $s = 250$ m, with permittivity $\varepsilon = 1.8$, a standard deviation of time measurements $\Delta T = 10$ ns**,** and an accuracy of $\Delta s = 6$ m (standard deviation of positioning on the orbit), we obtained $\Delta\varepsilon/\varepsilon = 0.05$, which gives $\Delta\varepsilon = 0.1$.

For longer travel distances, e.g. $s = 1000$ m**,** with eps $= 1.4$**,** the accuracy is $\Delta\varepsilon/\varepsilon = 0.013$, which gives $\Delta\varepsilon = 0.018$.

The error in permittivity for short travel distances of the wavefront inside the comet, is of the order of 0.1, and for long distances ~0.018.

This paper has been typeset from a Microsoft Word file prepared by the author.